Tilt-related alignment issues in miniature micromechanical on-wafer electrical probes composed of multiple flexible microcantilevers

Steve Arscott

DOI: 10.1088/2631-8695/ad2ccc

Tilt-related alignment issues in miniature micromechanical on-wafer electrical probes composed of multiple flexible microcantilevers

Steve Arscott

University of Lille, CNRS, Centrale Lille, Univ. Polytechnique Hauts-de-France, UMR 8520-IEMN, F-59000 Lille, France.

E-mail: steve.arscott@univ-lille.fr

https://orcid.org/0000-0001-9938-2683

Abstract

Some new issues concerning the contacting and positioning of small electrical microelectromechanical systems (MEMS) probes based on multiple, flexible microcantilevers are presented here. A tilt error, associated with the lateral probe roll, means that contact touchdown occurs sequentially in different cantilevers upon increasing probe overtravel. To understand the relationship between probe overtravel, tip skate, tip planarity, tip tangency, and contact force in the different contacts, the relationship between mechanical bending and torsion of the flexible cantilevers needs to be accounted for. The study reveals the conditions for achieving contact planarity and desired contact force, as well as the identification of a new 'differential skate error' contact misalignment associated with such MEMS probes based on multiple, flexible microcantilevers. This misalignment leads to a 'differential contact force error' which has implications for electrical contact quality. An experimental scale model probe based on three cantilevers is used to test the modelling—the results agree well with the predictions of the model. Interestingly, the experiments revealed an effect not accounted for in the modelling; this 'twist error' resulted in the cantilever lead edge not being parallel to the touchdown plane. The findings may be useful for engineers involved with the automatic control positioning of such emerging miniature probes, especially in terms of the impact of probe positioning errors.

1. Introduction

Microfabrication and microelectromechanical systems (MEMS) approaches can be applied to miniaturize, functionalize, and innovate the architecture of high-frequency probes [1,2], thus meeting the challenges of on-wafer measurements of shrinking electronics working at higher and higher frequencies [3–5]. The use of such miniature probes, based on flexible microcantilevers, means that

new challenges arise compared to their rigid counterparts. One of these challenges is an understanding of the link between the positioning of such probes and their inherent mechanical flexibility. This is particularly important in terms of the impact of positional errors on optimum electrical contact [6]; something that has been studied in rigid commercial probes [7–14]. In contrast, the micromechanical behaviour (bending and twisting) of miniature microcantilever-based probes must be taken into account for optimum probe contacting [15–17]. The author has previously discussed the relationship between skate and overtravel in rectangular [15], triangular, and trapezoid [16] shaped probes based on flexible microcantilevers. The impact of tilt error on a probe composed of a single flexible microcantilever has also been described by the author [17]. This work revealed interesting aspects such as: probe tip planarity and tangency, the possibility of zero-skate probing, contact force issues, and the interplay between the bending and torsional stiffnesses of single cantilever-based probes.

This paper describes geometrical issues concerning the contacting of a micromechanical probe, based on more than one flexible cantilevers, in the presence of a tilt error. The example of a three-contact probe, akin to the well-known ground-signal-ground (GSG) microwave probe, is used to illustrate the ideas presented here. First, this paper gives a qualitative description of the problem. Following this, a quantitative description of the problem is given based on analytical modelling—this enables prediction of the micromechanical behaviour of the probes. Finally, some experimental work is given using a scale model probe and compared with the model. The analytical model will help engineers understand and predict the impact of tilt errors on the automatic positioning and contacting of such probes [18,19].

2. Qualitative description of the problem

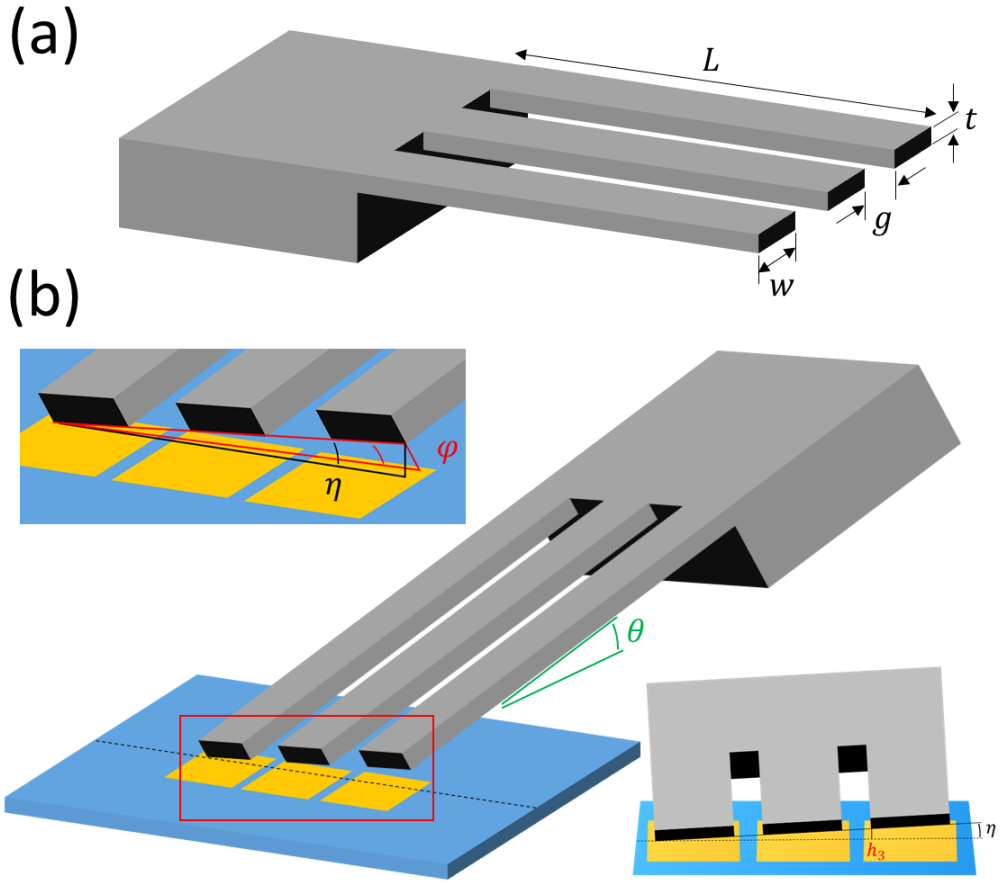

Figure 1. Schematic diagrams showing a three-contact electrical probe based on three flexible microcantilevers. (a) Dimensions and (b) the tilt error. The probe has a tilt error angle φ in the roll axis. When the lower cantilever comes into contact with the surface, the perpendicular angle is η.

Figure 1(a) shows a probe based on three flexible cantilevers (grey) having dimension length L, width w, gap g, and thickness t. The three cantilevers are attached to a rigid support chip. The cantilevers are inclined at a certain angle with respect to the surface, termed the probe angle θ. Let us consider the probe approaching an underlying surface (blue) by imposing a vertical downward movement (known as probe 'overtravel') to the support chip. In the presence of a tilt roll error φ [17], i.e. the cantilever tip edges not being parallel to the approaching underlying surface, the lower bottom corner of the lowest cantilever edge will make contact with the surface first. Following touchdown, the imposition of further overtravel will have two consequences: (i) to cause the lower corner of the cantilever to bend and skate along the surface and (ii) to cause the cantilever to twist. Depending on the values of the bending stiffness and the torsional stiffness of the cantilevers, three main scenarios can be identified as further vertical overtravel is imposed. These are described in the following subsections.

2.1 Sequential touchdown and tip planarity

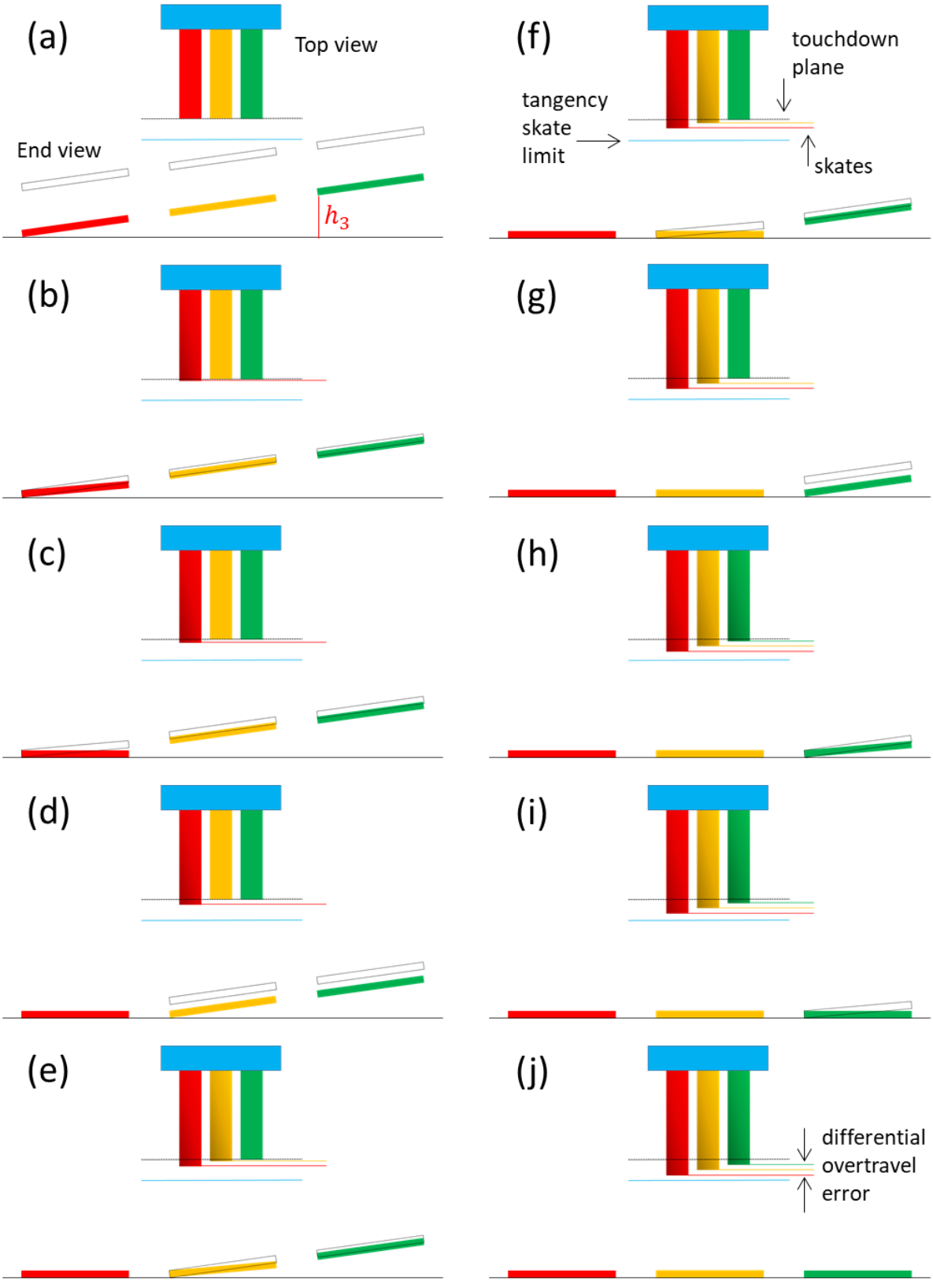

Figure 2. Schematic diagram showing a probe based on three flexible cantilevers approaching an underlying surface upon imposing a downward overtravel: the case of sequential touchdown and tip planarity. The stages (a) to (j) show the sequence of contacting from touchdown (a) to planarity of all

three cantilever tips (j). The upper images show top views of the cantilevers indicating the resulting tip skate at each stage. The horizontal dashed black line indicates the touchdown plane. The horizontal solid blue line indicates the tangential skate of the red cantilever. The horizontal red, yellow, and green lines represent the progression of the skate of each cantilever tip. Note that the gradient effect on the colours of the cantilevers indicates mechanical bending and torsion of the cantilever.

Figure 2 shows a probe based on three cantilevers (red, yellow, and green) attached to a rigid support (light blue) being brought into contact with an underlying surface (long horizontal black line) in the presence of a tilt error associated with the roll axis of the probe. Each image is composed of a top view of the probe (upper images) and an end view of the cantilevers (lower images). In Figure 2 the short horizontal dashed black lines in the upper images indicate the initial contact or 'touchdown' plane, the horizontal solid blue line indicates the tangential skate of the red cantilever, and the horizontal red, yellow, and green lines represent the progression of the skate of each cantilever tip as the overtravel is increased. Note that the gradient effect on the colours in Figure 2 indicates mechanical bending and torsion of the cantilever.

The sequence starts with touchdown of the lowest cantilever (red)—Figure 2(a). At a given value of overtravel, twisting of the cantilever brings the whole of the lower edge of the first cantilever into contact with the surface—Figure 2(c). This is the planarity overtravel of a single skating inclined cantilever [17]. Subsequently, further overtravel will now have two consequences: (i) further skating of the lower cantilever (red) along the surface (associated with an increase of its contact force with the surface due to increased bending) and (ii) a repeat of the process described above with the middle cantilever (yellow), i.e. corner contact followed by skating, twisting, and planarity—Figure 2(f). Evidently this is followed by the next cantilever (green) making contact with the surface and repeating the process whilst the first two cantilevers (red and yellow) skate further along the surface, their contact forces increasing as overtravel causes increased bending of the cantilevers. Eventually, the third cantilever (green) also achieves planarity—Figure 2(i). It should be noted that for this example, all three cantilever tips achieve planarity with the surface before the first cantilever (red) achieves tangency [15] with the surface. Figure 2(j) indicates that in this scenario further skate (and increased contact force) can be obtained without reaching the tangential skate of the red cantilever—indicated by the solid blue line in Figure 2.

This reasoning enables us to see that for a given roll error angle, a given geometry, and mechanical properties of the cantilever material, there will be an overtravel that brings all three cantilever edges into contact with the surface (planarity) and also an overtravel which results in a

certain contact force on the cantilever edges—although this will vary from cantilever to cantilever as the bending is different. Note that the value of the cantilever skates will also be different. Depending on the roll error angle, the skate of the lower cantilever (which makes contact with the surface initially) will be larger than the skate of the second cantilever, which is greater than that of the third cantilever—Figure 2(j). The skates of the three cantilevers will thus be staggered if there is a tilt error associated with roll. We can call this difference—between the leading cantilever edge and the last cantilever edge—the 'differential skate error' or 'DSE'. One can anticipate that the main consequences of this differential skate error are: (i) a probe/contact misalignment and (ii) a 'differential contact force error' or 'DCFE' between different cantilevers and contact pads—this is potentially important as contact force determines contact resistance in metal/metal contacts [20].

2.2 Touchdowns occur before planarity

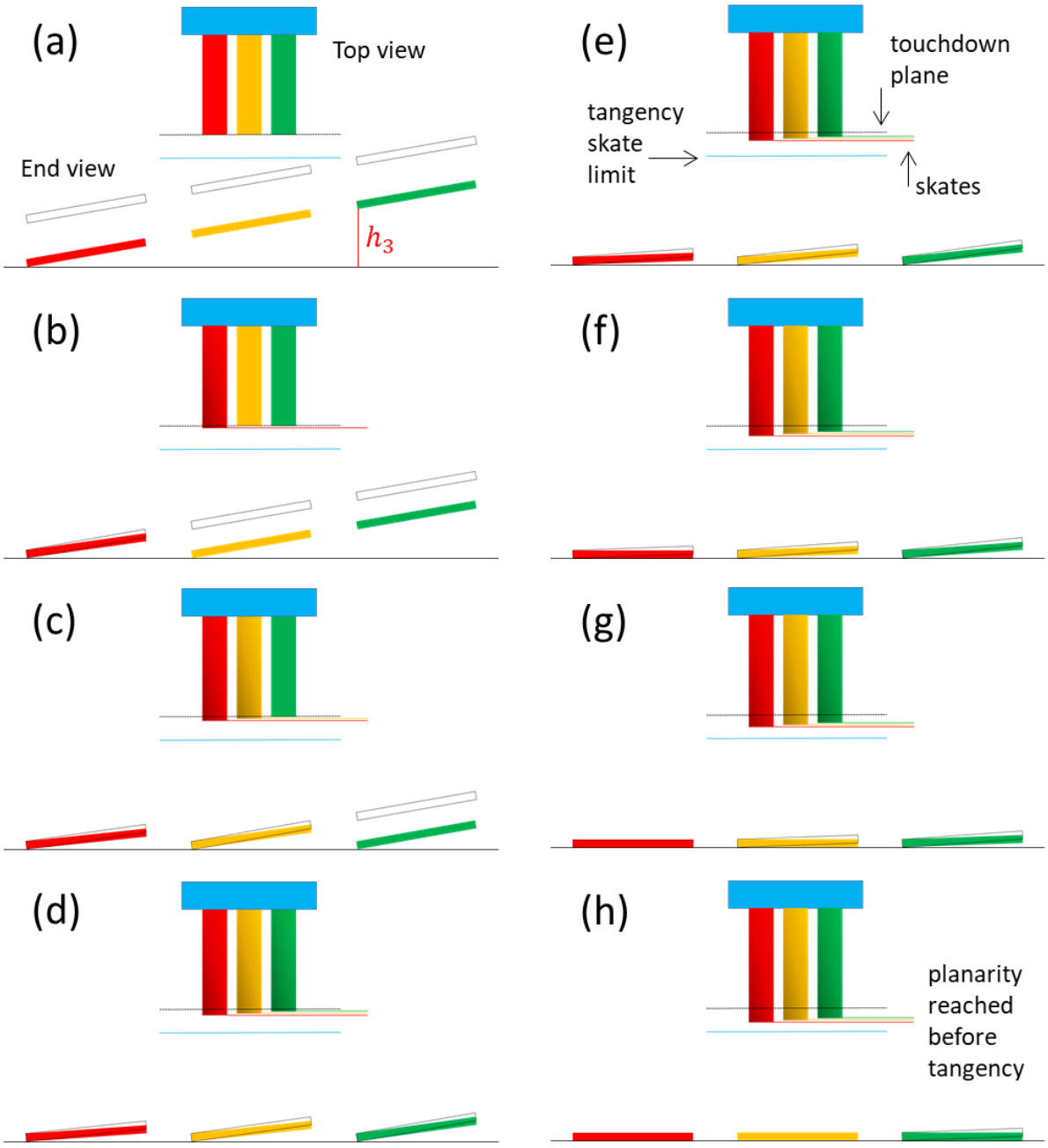

Figure 3. Schematic diagram showing a probe based on three flexible cantilevers approaching an underlying surface upon imposing a downward overtravel: case where touchdowns occur before planarity. The stages (a) to (h) show the sequence of contacting from touchdown (a) to planarity of all three cantilever tips (h). The upper images show top views of the cantilevers indicating the resulting tip skate at each stage. The horizontal dashed black line indicates the touchdown plane. The horizontal solid blue line indicates the tangential skate of the red cantilever. The horizontal red, yellow, and green lines represent the progression of the skate of each cantilever tip. Note that the gradient effect on the colours of the cantilevers indicates mechanical bending and torsion of the cantilever.

Figure 3 shows a scenario where all cantilevers enter into touchdown before tip planarity is achieved. Again, we can consider a probe is based on three cantilevers (red, yellow, and green) attached to a rigid support (light blue) being brought into contact with an underlying surface (long horizontal black line) in the presence of a tilt error associated with the roll axis of the probe. Each image is composed of a top view of the probe (upper images) and an end view of the cantilevers (lower images). In Figure 3 the short horizontal dashed black lines in the upper images indicate the initial touchdown plane, the horizontal solid blue line indicates the tangential skate of the red cantilever, and the horizontal red, yellow, and green lines represent the progression of the skate of each cantilever tip as the overtravel is increased. Note that the gradient effect on the colours in Figure 3 indicates mechanical bending and torsion of the cantilever.

The probe is initially brought into contact (touchdown)—Figure 3(a). Probe overtravel results in the other two cantilevers (yellow and green) achieving touchdown before the first cantilever (red) achieves planarity. Finally, a certain overtravel results in all cantilevers achieving planarity—Figure 3(h). Note that planarity of the third cantilever (green) is achieved before the tip tangency condition [15] is arrived at for the first (red) cantilever—indicated by the horizontal blue line in Figure 3. This scenario shown in Figure 3 also results in a DSE between the laterally advancing tips and a DCFE.

2.3 Tip tangency achieved before planarity

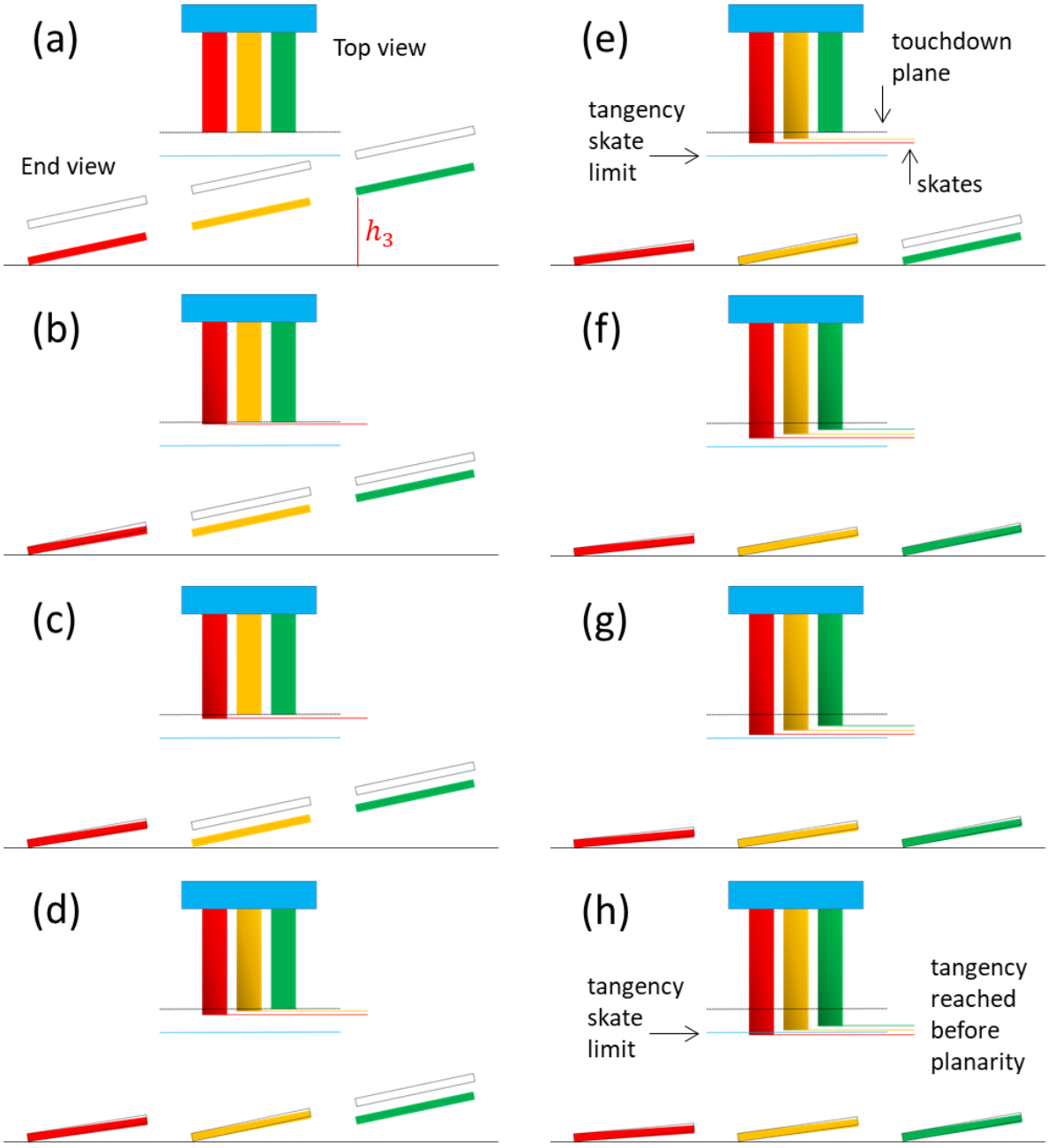

Figure 4. Schematic diagram showing a probe based on three flexible cantilevers approaching an underlying surface upon imposing a downward overtravel: case where tip tangency occurs before planarity. The stages (a) to (h) show the sequence of contacting from touchdown (a) to tangency of the first (red) cantilever tip (h). The upper images show top views of the cantilevers indicating the resulting tip skate at each stage. The horizontal dashed black line indicates the touchdown plane. The horizontal solid blue line indicates the tangential skate of the red cantilever. The horizontal red, yellow, and green lines represent the progression of the skate of each cantilever tip. Note that the gradient effect on the colours of the cantilevers indicates mechanical bending and torsion of the cantilever.

Figure 4 shows a probe contact scenario where tip planarity is never reached due to high torsional stiffness of the cantilevers. This occurs because tip tangency [15] of the first cantilever is achieved before planarity [17]. Again, we consider a probe based on three cantilevers (red, yellow, and green) attached to a rigid support (light blue) being brought into contact with an underlying surface (long horizontal black line) in the presence of a tilt error associated with the roll axis of the probe. Each image is composed of a top view of the probe (upper images) and an end view of the cantilevers (lower images). In Figure 4 the short horizontal dashed black lines in the upper images indicate the initial contact plane, the horizontal solid blue line indicates the tangential skate of the red cantilever, and the horizontal red, yellow, and green lines represent the progression of the skate of each cantilever tip as the overtravel is increased. Note again that the gradient effect on the colours in Figure 4 indicates mechanical bending and torsion of the cantilever.

Again, the probe makes contacts with the underlying surface where the lowest cantilever (red) makes touchdown—Figure 4(a). As above, there is a sequence of contacting as the overtravel is increased. Eventually, all cantilevers will be in contact with the surface—Figure 4(e). However, further overtravel results in the first cantilever (red) achieving tip tangency before it achieves planarity. This situation is shown in Figure 4(h) where the tip skate of the red cantilever has gone beyond the horizontal blue line (the tangency skate of the red cantilever). In this case, increasing the overtravel beyond the tangency overtravel value [15,16] may cause the tips to leave the surface, jeopardizing electrical contact quality.

Let us now try to use analytical modelling, along with some assumptions, to try to find relationships between the different parameters of the system described above. By describing the probe quantitatively, engineers will be able to predict probe behaviour using some simple equations. Analytical modelling can also sometimes reveal unforeseen behaviour—some of which can be counterintuitive, as we shall see.

3. Quantitative description using analytical modelling

Figure 1(a) shows dimensions and angles considered in the modelling. In order to develop a mathematical model of the situation qualitatively described above, let us again consider a three-contact probe composed of three flexible, rectangular microcantilevers. The term microcantilever implies that any bending due to gravity (typically 10^{-9} N) is negligible. Each cantilever has dimensions length L, width w, and thickness t. Also, the cantilevers of the probe are separated by a gap g. The

cantilever material has a Young's modulus E, a shear modulus G (associated with torsion), and a Poisson ratio ν where:

$$\nu = \frac{E}{2G} - 1 \tag{1}$$

We can consider that the cantilevers are inclined to have a probe angle θ—as shown in Figure 1(b). We also consider that they are initially straight and attached to a rigid mounting—this could be another part of the probe, e.g. a support chip. Let us assume that the cantilevers have a roll error angle given by φ—as indicated in Figure 1(b). The vertical downward overtravel of the probe is δ and the probe cantilever skate is Δ. Note that in the presence of tip/surface friction, a first approximation of the condition for tip skate is [15,21]:

$$\tan\theta \leq \frac{1}{\mu} \tag{2}$$

Where θ is the probe angle (see above) and μ is the coefficient of friction between the probe tip and surface materials. Note that beyond friction, other potential cantilever/surface interactions [22] are not considered in the current model, but could be accounted for if necessary.

For a probe based on n cantilevers, upon touchdown of the lower corner of the lowest cantilever, the lower corner of the n^{th} cantilever is a perpendicular distance h_n from the underlying surface equal to:

$$h_n = (n-1)(w+g)\sin\eta \tag{3}$$

Where the angle η—see Figure 1(b)—is related to the probe angle θ and the roll error angle φ by:

$$\eta = \varphi\cos\theta \tag{4}$$

Imposition of an overtravel $\delta = h_n$ brings the lower corner of the n^{th} cantilever into contact with the underlying surface.

In addition to this, for a rectangular cantilever having a roll error φ, the tip deflection d_p required to achieve planarity is given by [17]:

$$d_p = \frac{4L^2 J\varphi}{(1+\nu)w^2t^3} \tag{5}$$

Where the torsional constant J of a rectangular beam is given by [23]:

$$J = wt^3\left[\frac{1}{3} - 0.21\frac{t}{w}\left(1 - \frac{t^4}{12w^4}\right)\right] \tag{6}$$

Note that this is the deflection d_p of the cantilever *perpendicular to the probe angle* θ, not to be confused with the vertical overtravel δ.

For a cantilever inclined at an angle θ, the vertical overtravel δ, the deflection d, the lateral tip deflection d_x, and the bending angle of the cantilever α are related by the following three equations [15]:

$$\delta = d\cos\theta + d_x \sin\theta \tag{7}$$

$$d_x = fL\left(1 - \sqrt{\frac{\sin\alpha}{\alpha}}\right) \tag{8}$$

$$\alpha = \frac{3d}{2L} \tag{9}$$

Where f is a constant (experimentally determined to be 3.3 for a rectangular cantilever [15]), d_x is the lateral movement of the tip of a fixed-free rectangular cantilever beam with a concentrated load at the free end under both small and large deflection [15], and α is the bending angle of the cantilever. Let us remember that the tip deflection d is perpendicular to the angle of inclination θ of the probe, i.e. at an angle θ to the direction of the vertical overtravel δ. These three equations can be solved numerically to obtain the value of deflection d corresponding to a given overtravel δ.

In addition, the skate Δ of the cantilever along the underlying surface is given by [15]:

$$\Delta = \delta\tan\theta - \frac{d_x}{\cos\theta} \tag{10}$$

The tangency overtravel δ_T of a tilted rectangular cantilever is given by [15]:

$$\delta_T = \frac{2L\theta}{3}\cos\theta + fL\sin\theta\left(1 - \sqrt{\frac{\sin\theta}{\theta}}\right) \tag{11}$$

This condition occurs when the bending angle α of the cantilever equals the probe angle θ.

Finally, the contact force of the cantilever $F_{contcat}$ (perpendicular to the surface), which depends on the individual deflection d of each cantilever, is given by [15,21]:

$$F_{contcat} = \frac{dEwt^3}{4L^3\cos\theta} \tag{12}$$

At this point we are able to calculate the skates and contact forces of each cantilever in the presence of a tilt error. Let us take the example of a simple probe based on three cantilevers to make some interesting predictions. Note that electromagnetic issues related to the probe materials, dimensions, and geometry are not considered at the moment.

In the following section I will describe step-by-step how the analytical modelling is done to obtain the following graphs. Note that the overtravel is composed of three parts: (i) overtravel to make last contact touchdown, (ii) an extra overtravel to the make last contact planar with surface, and (iii)

an extra overtravel to achieve the desired contact force on last contact. The imposition of this overtravel will produce three different skate values and three different average contact force values in the three cantilevers.

First, we have a number of inputs (L, w, t, g, n, θ, φ, E, ν) which describe the probe. Second, the perpendicular angle η is computed using Equation 4. Third, the vertical height of the n^{th} contact is computed using Equation 3. Fourth, the *deflection* required to achieve planarity at the end of the cantilever (due to torsion) is computed using Equation 5. Fifth, the *overtravel* required to achieve planarity at the end of the cantilever (due to torsion) is computed using equation 7. Sixth, the individual overtravel values of each cantilever are computed by adding the overtravel required to achieve planarity to the vertical height of each cantilever before overtravel is imposed. Seventh, the *deflection* (d and the lateral d_x) of the n^{th} cantilever is computed by numerically solving Equations 7 and 8 above. The deflection d enables a computation of the contact force of each cantilever using Equation 12—this enables the differential contact force error (DCFE) to be computed. Eighth, the individual skate of each of the cantilevers is computed using Equation 10—this enables the DSE to be computed. Note that this current situation is the result for an imposed overtravel to bring the n^{th} cantilever into contact planarity with the surface. In addition, the overtravel required for this situation must be less than the overtravel required to achieve the tangency condition at the end of the lower cantilever—Equation 11. It is possible now to impose more overtravel to the system. This may be necessary to achieve a desired contact force on the n^{th} cantilever. In other words, the overtravel required for planarity on the n^{th} cantilever may not result in enough contact force for a good electrical contact [6].

The modelling permits this to be done—but the computed overtravel to cause a required contact force on the n^{th} cantilever must be less than the overtravel to cause tangency of the first, and lowest, cantilever. Let us now chose some practical dimensions of a 3-cantilever, silicon-based probe to predict some results of the modelling.

3.1 Effect of probe angle

In this part the modelled probes have the following dimensions: L = 250 µm, w = 50 µm, t = 5 µm, and g = 30 µm. The cantilevers are considered to be made of crystalline silicon [011] (E = 169 GPa, ν = 0.065). The probe angle θ was varied from 20° to 45°. The roll error angle φ was varied from 0.5° to 2°. The modelling demonstrates how the contact force of each cantilever varies, how the skate of each cantilever varies, and how the DSE varies.

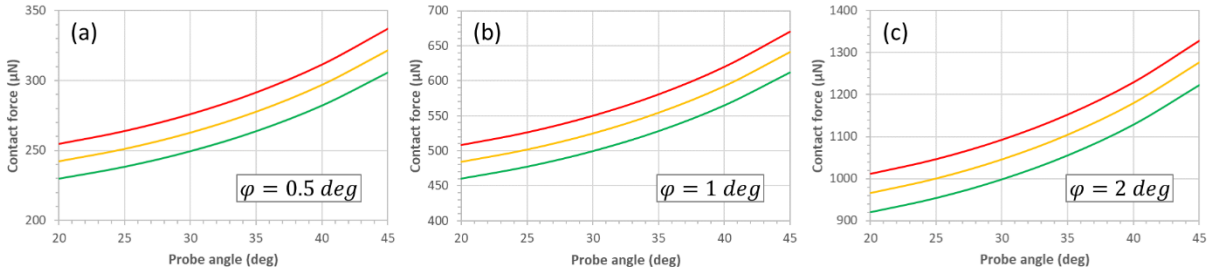

Figure 5. Variation of the contact force of each cantilever (red, yellow, and green) of the probe as a function of probe angle θ and tilt roll error angle φ. (a) φ = 0.5°, (b) φ = 1°, and (c) φ = 2°. The cantilever dimensions of the probe are: L = 250 μm, w = 50 μm, t = 5 μm, and g = 30 μm.

Figure 5 shows how the contact force of each of the three cantilevers (red, yellow, and green) varies with probe angle and roll error angle. The three values of force correspond to when the whole of the edge of the final cantilever (green) comes into contact with the surface after imposed overtravel causes tip skating. First, for a given roll error angle, the contact force on each cantilever increases nonlinearly with probe angle. Second, the DSE caused by the roll error is predicted to be constant as the probe angle is varied.

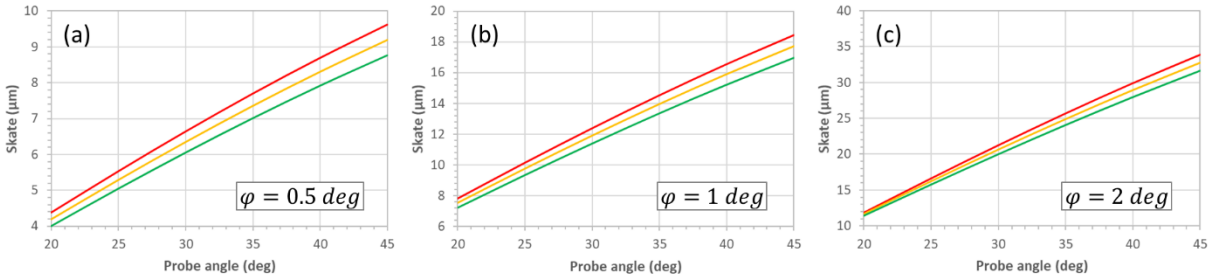

Figure 6. Variation of the skate of each cantilever (red, yellow, and green) of the probe as a function of probe angle θ and tilt roll error angle φ. (a) φ = 0.5°, (b) φ = 1°, and (c) φ = 2°. The cantilever dimensions of the probe are: L = 250 μm, w = 50 μm, t = 5 μm, and g = 30 μm.

Figure 6 shows how the ultimate skate of each cantilever (red, yellow, and green) varies with probe angle and roll error angle. The ultimate skate is the skate induced by bringing the last cantilever (green) into parallel contact with the surface by imposing an overtravel. First, the ultimate skate increases in a quasi-linear way with increasing probe angle. Second, the difference in the skates of the three cantilevers (red, yellow, and green) increases as the probe angle is increased—this is the DSE.

Note that these skates are the values obtained when the tip of final cantilever (green) is planar to the surface.

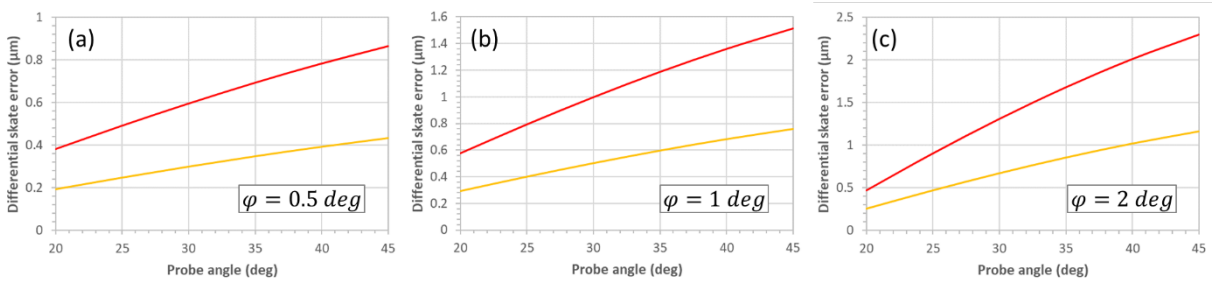

Figure 7. Variation of the differential skate error of the red and yellow cantilevers compared to the green cantilever as a function of probe angle θ and tilt roll error angle φ. (a) φ = 0.5°, (b) φ = 1°, and (c) φ = 2°. The cantilever dimensions of the probe are: L = 250 µm, w = 50 µm, t = 5 µm, and g = 30 µm.

Figure 7 plots the variation of the DSE as a function of probe angle and roll error angle. The DSE is obtained by subtracting the values of the ultimate skate of each cantilever (red, yellow, and green) in Figure 6. Thus, in Figure 7 the red curves correspond the how much the red cantilever skate is ahead of the green cantilever, and the yellow curves correspond the how much the yellow cantilever skate is ahead of the green cantilever. The DSE increases with probe angle. The difference between the DSE of the two leading cantilevers (red and yellow) increases with probe angle. The DSE increases with roll angle error.

3.2 Effect of geometry

In this part the modelled probes have the following dimensions: L = 125-250 µm, w = 50 µm, t = 5 µm, g = 30 µm, θ = 25°. The cantilevers are again considered to be made of crystalline silicon. The cantilever length L was varied from 125 µm to 250 µm in order to see the effect of variable cantilever stiffness. The tilt roll error angle φ was increased from 0° until the condition were tip tangency is not possible. The modelling resulted in how the contact force of each cantilever varied, how the skate of each cantilever varied, and how the DSE varies.

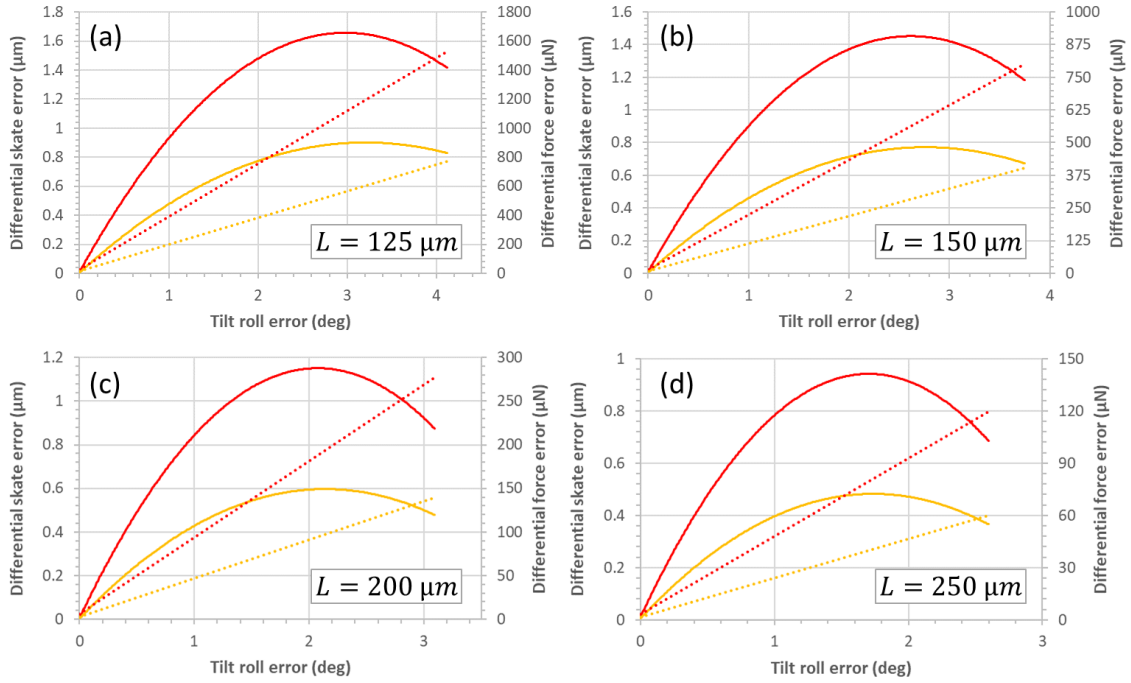

Figure 8. Variation of the differential skate error (solid lines) and the differential contact force error (dashed lines) of the red and yellow cantilevers compared to the green cantilever as a function of probe length L and tilt roll error angle φ. (a) L = 125 µm, (b) L = 150 µm, (c) L = 200 µm, and (d) L = 250 µm. The other cantilever dimensions of the probe are: w = 50 µm, t = 5 µm, and g = 30 µm. The probe angle θ is fixed at 25°.

Figure 8 shows the variation of the DSE and the DFE for the two leading cantilevers (red and yellow) of a three-cantilever probe as a function of tilt roll error and cantilever length. Interestingly, there is a maximum DSE as the tilt roll error angle is increased. For a given roll error angle, the DSE decreases as the cantilever length is increased (decreasing cantilever stiffness). There is a maximum tilt roll error angle – this is where tip planarity of one or more of the cantilever tip cannot be achieved due to the leading cantilever achieving tangency with the surface—as schematically indicated in Figure 4. For example, when L = 125 µm, the maximum roll error angle is 4.1°. The DCFE increases linearly with roll error angle—and decreases as the cantilever length increases (stiffness decreasing).

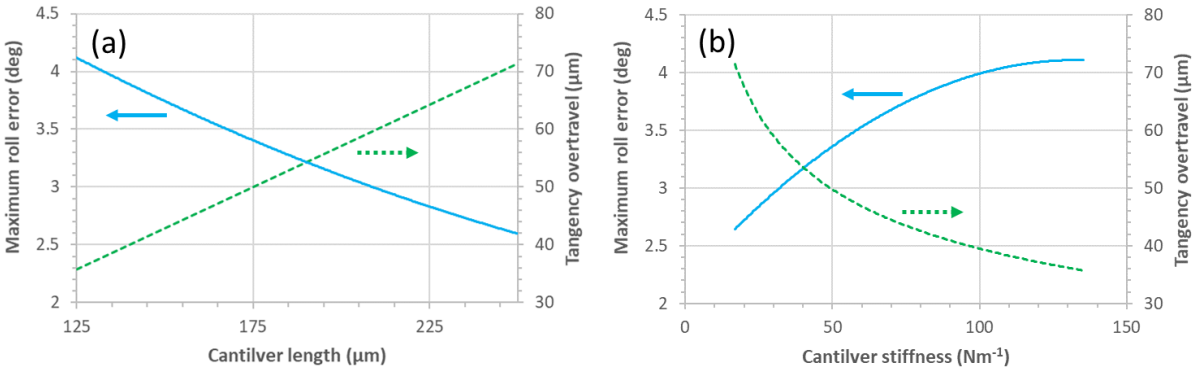

Figure 9. Variation of the maximum roll error angle (solid lines) and the tangency overtravel for a probe based on three microcantilevers. (a) As a function of cantilever length L, and (b) as a function of cantilever stiffness. The cantilever dimensions of the probe are: L = 125-250 µm, w = 50 µm, t = 5 µm, and g = 30 µm. The probe angle θ is fixed at 25°.

Figure 9 shows how the maximum allowable roll error angle and the tangency overtravel vary as a function of cantilever length and stiffness. As the cantilever length increases and the stiffness reduces, the maximum roll error angle decreases.

4. Experimental validation of the model

4.1 Fabrication and Experimental setup

A scale model of a probe based on three rectangular cantilevers was fabricated for the study using thin, dense polystyrene sheets (Schulcz GmbH, Germany). The thickness of the polystyrene was measured to be 1.45±0.01 mm using a precision thickness gauge (Mitutoyo, Japan) having a resolution of 1 µm. The Young's modulus of and Poisson coefficient the polystyrene has been determined by the author to be 1.754±0.071 GPa and 0.33 [16,17]. The design dimensions of the scale model probe are: L = 100 mm, 75 mm, and 50 mm, w = 25 mm, and g = 15 mm. The details of the fabrication of such objects can be found in previous publications [16,17]. Following fabrication, the width of the cantilevers and the gap length were measured from photographs using software [24]. This gave a value of w = 24.98±0.21 mm and g = 14.85±0.20 mm for the width and the gap. The error on the cantilever length in the setup is estimated at ±0.5 mm, this corresponds to a 1% error.

The experimental setup was similar to that described in detail in previous work [17]. First, the cut polystyrene cantilever scale model is mounted onto the tool—see Figure 10(a). This mounting enables the cantilever length L to be set. Second, the tilt angle φ is set to zero by setting the

perpendicular angle η to zero. The tool is then moved forward so that all cantilevers make contact with the surface. A photograph is taken of this configuration and image analysis enables the touchdown plane to be identified. Third, a tilt angle is applied to the tool. The applied perpendicular angle η is verified by taking a photograph from the top view of the tool—see Figure 10(b). The tool is then moved forward until planarity of the third cantilever is observed. The overtravel δ is recorded in this configuration and a photograph is taken of the cantilevers. Image analysis [24] of this photograph enables the skate Δ and the DSE to be evaluated.

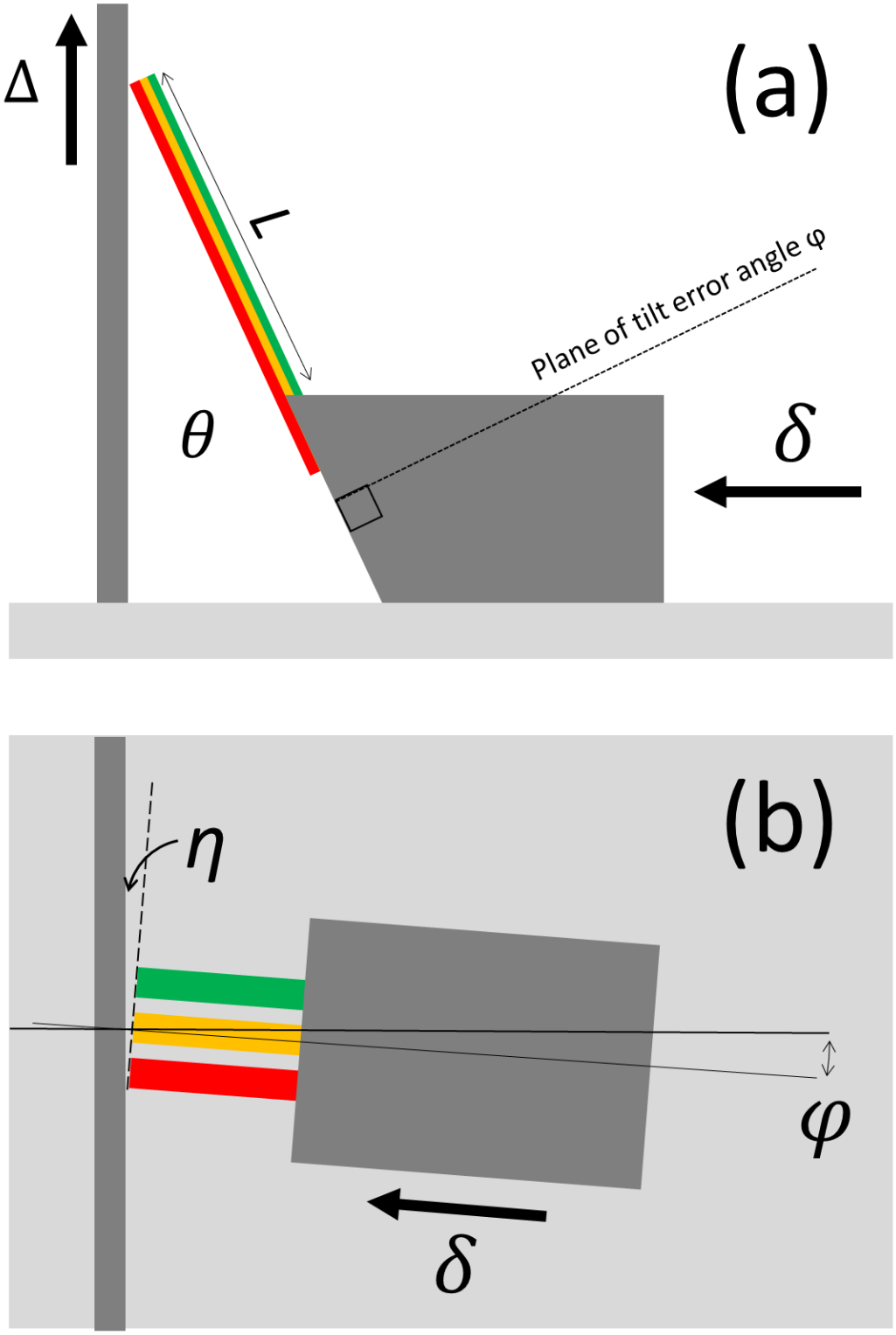

Figure 10. Schematic diagram of the experimental setup: (a) side view and (b) top view. The dashed black line in (a) indicates the rotation plane of the tilt angle φ. The tilt error angle φ is computed from the observed perpendicular angle η [17].

4.2 Experimental results

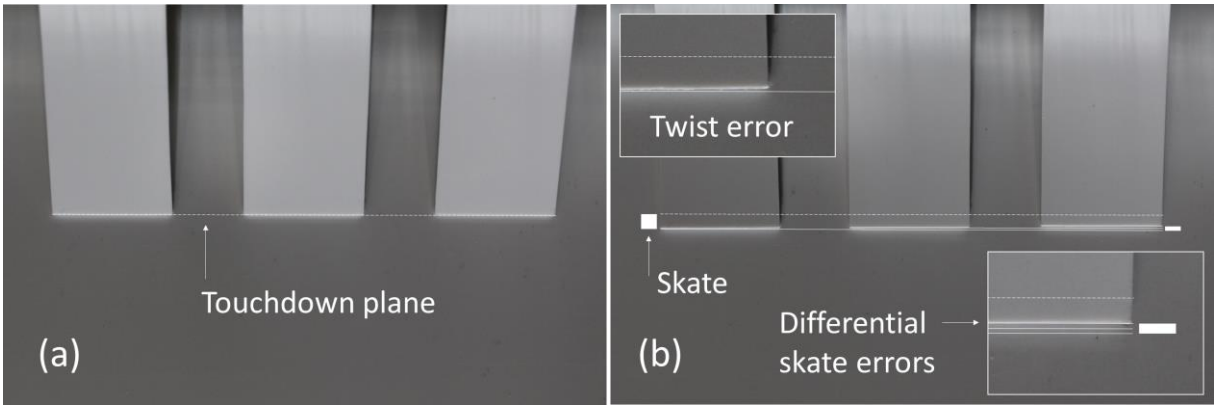

Figure 11. Experimental skate of a scale model probe based on three cantilevers. The tilt error angle φ is 4.5°. (a) The probe in contact with the surface for zero tilt error; the touchdown plane is illustrated by the horizontal dashed white line. (b) The probe with all cantilever ends planar to the surface. The upper inset to (b) shows the experimental twist error. The lower inset to (b) shows the experimental differential skate errors. The touchdown plane is reproduced in (b) to illustrate the probe skate and differential skate errors (shown by the horizontal white lines). The cantilevers have the following design dimensions: L = 50 mm, w = 25 mm, t = 1.5 mm, and g = 15 mm. The probe angle θ is 25°.

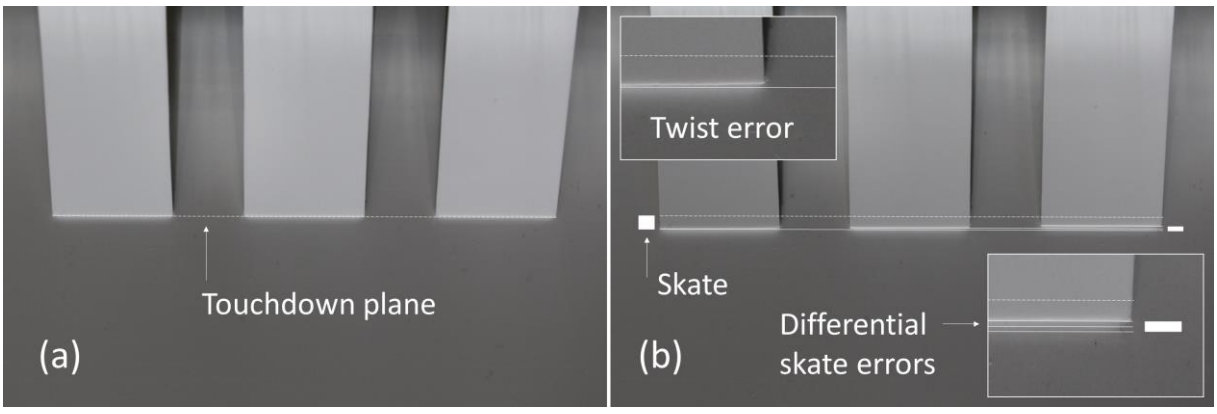

Figure 12. Experimental skate of a scale model probe based on three cantilevers. The tilt error angle φ is 3.3°. (a) The probe in contact with the surface for zero tilt error; the touchdown plane is illustrated by the horizontal dashed white line. (b) The probe with all cantilever ends planar to the surface. The upper inset to (b) shows the experimental twist error. The lower inset to (b) shows the experimental differential skate errors. The touchdown plane is reproduced in (b) to illustrate the probe skate and

differential skate errors (shown by the horizontal white lines). The cantilevers have the following design dimensions: L = 50 mm, w = 25 mm, t = 1.5 mm, and g = 15 mm. The probe angle θ is 25 deg.

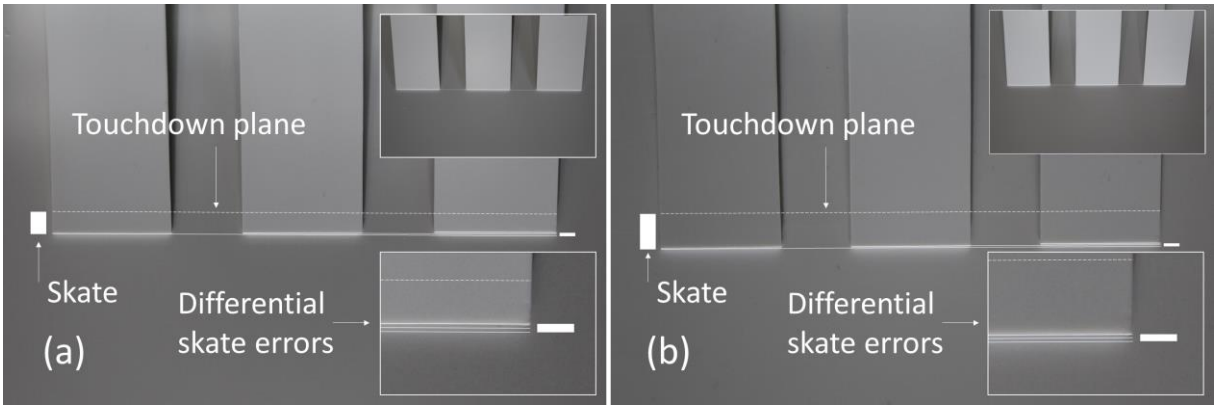

Figure 13. Experimental skate of a scale model probe based on three cantilevers. The tilt error angle φ is 3.3° deg. (a) A probe having a cantilever length L = 75 mm; the touchdown plane is illustrated by the horizontal dashed white line. (b) A probe having a cantilever length L = 100 mm; the touchdown plane is illustrated by the horizontal dashed white line. The top insets to (a) and (b) show the touchdown planes of the probe. The bottom insets to (a) and (b) show the experimental differential skate errors, illustrated by the horizontal white lines. The cantilevers have the following design dimensions: w = 25 mm, t = 1.5 mm, and g = 15 mm. The probe angle θ is 25°.

Figure 11, Figure 12, and Figure 13 show optical images of the experimental skate of the scale model probes. Figure 11 was obtained at a tilt error angle experimentally determined to be 4.5°. Figure 12 and Figure 13 were obtained at a tilt error angle experimentally determined to be 3.3°. In the current setup, the experimental tilt angle error is estimated at ±0.2°. The overtravel error is estimated to be ±0.2mm.

Figure 11(a) and Figure 12(a) show the touchdown plane of the scale model probes for a tilt error of 0°. Figure 11(b) and Figure 12(b) show the scale model probe cantilever tips in planarity with the vertical surface—in all cases the computed tangential planarity [15] is not exceeded. The skate is indicated by the larger white rectangle. The insets to Figure 11(b) and Figure 12(b) are zoomed images showing the DSE, indicated by horizontal white lines. The difference between the upper and lower solid white lines is indicated by the smaller white rectangle—this is the DSE. In all cases the touchdown plane of the scale model probe is indicated by the dashed white lines.

Let us consider Figures 11, 12, and 13 and compare them. First, it is apparent that the predicted DSE is visible in the images. This is the difference between the horizontal solid white lines in insets to the figures. Note that care was taken to avoid image rotation errors from photograph to photograph by analysing defects visible on the vertical surface. This ensures that any observed DSE is real rather than an artefact generated by an image rotation error—this is important as the DSE are relatively small, even in this macroscopic setup. Second, for a constant tilt error angle, it is observed that the skate increases as the cantilever length increases. This is the difference between the horizontal dashed white lines (touchdown plans) and the horizontal solid white line. Third, for a constant tilt error angle, it is observed the DSE increases as the cantilever length reduces. Fourth, planarity of the final cantilever (rightmost in the images) is achieved for a given overtravel, which increases with increasing cantilever length. Finally, for a constant cantilever length, when the tilt error angle is increased, the skate and required planarity overtravel both increase but the DSE does not significantly change.

Interestingly, a small effect is observed in the data which is not predicted by the model. When in planarity, the leading edges of the cantilevers are no longer precisely parallel to the original touchdown plane. We can call this the 'twist error' of a single cantilever. This is indicated in upper insets to Figure 11 and Figure 12. Again, by ensuring no rotation error, the magnitude of this small effect can be measured to be approximately 350 μm for a cantilever length of 50 mm. It can be explained in the following way. Due to the tilt error, the touchdown corner of one cantilever is nearer the vertical surface than the other. This means that when the deflected, twisted cantilever is in contact planarity with the surface then its shape adjusts to cause this effect. As the current analytical model cannot account for this, numerical modelling would be more appropriate to investigate this.

Table 1 give a summary of the experimental results. The skate and the DSE are averages given to three significant figures based on multiple measurements and analysis of the photographic data [24]. The photographs have a pixel size of 30 μm. In order to accurately extract the skate and the DSEs, the edge contrast of the cantilevers is enhanced by increasing the sharpness of the photographs. This is done by applying an algorithm using software [25,26]. Using these methods, the error on the average skate and the DSE is estimated to be ±50 μm.

Table 1. Summary of experimental results.

φ (°)	*L* (mm)	Overtravel δ (mm)	Skate Δ (mm)	Differential skate error (mm)
4.5	50	13.5	3.285	0.992

3.3	50	10.3	2.944	1.004
3.3	75	16.5	4.734	0.818
3.3	100	24	7.356	0.684

We can now compare the experimental results to those predicted by the model.

4.3 Comparison of results with modelling predictions

The predictions of the model are shown in Table 2. The values given in Table 2 are obtained by using the experimentally-determined dimensions and the scale model probe and the experimentally-determined mechanical properties of the polystyrene—see above.

Table 2. Summary of modelling predictions.

φ (°)	*L* (mm)	Overtravel δ (mm)	Skate Δ (mm)	Differential skate error (mm)
4.5	50	12.846	3.624	1.062
3.3	50	9.363	3.061	1.056
3.3	75	16.053	4.965	0.845
3.3	100	25.629	7.239	0.607

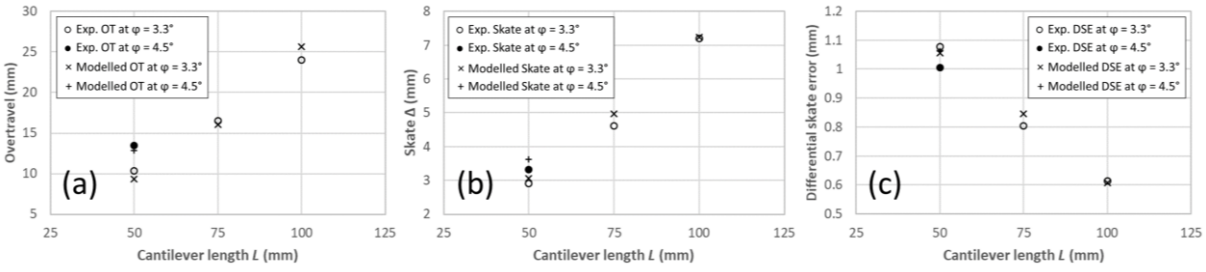

Figure 14. A comparison of the experimental results and the predictions of the model. (a) The overtravel, (b) the skate and (c) the differential skate error plotted as a function of cantilever length. Experimentally obtained values are in circles, values obtained from the modelling are in crosses.

Figure 14 plots the experimental overtravel, skate, and DSE obtained from the testing of the scale model probes; and compared this data with the predictions of the modelling presented in Section 3. First, the trends of the experimental data agree well with the predictions of the model: the skate increases with cantilever length and the DSE decreasing with increasing cantilever length. Second, the magnitudes of the experimental results agree well with the model predictions. One can see that if a small DSE is sought, a longer more flexible cantilever should be employed but at the expense of a larger skate. Finally, it would be interesting to repeat the methodology of such measurements on smaller microfabricated probes using other imaging methods for smaller dimension, e.g. scanning electron microscopy.

5. Conclusions

There is interesting relationship between the bending stiffness and the torsional stiffness of a microcantilever which determines how a probe composed of n such microcantilevers makes contact with a surface in the presence of a tilt error. Analytical modelling enables one to predict the micromechanical behaviour of these probes—the study has shown that the results are sometimes counterintuitive. The analytical modelling also enables general ideas to be understood which could, in principle, be extended to more specific complex probe geometries (e.g. other cantilever shapes) and modelled by numerical approaches to give useful engineering solutions. The analytical modelling has enabled several effects to be identified and quantified. First, the tilt error has an impact on the ultimate skate in the different cantilevers. A new 'differential skate error' or 'DSE' contact misalignment has been identified in such probes. In addition, if the skate error can be measured, the model enables the tilt error to be computed and compensated for. Second, the modelling predicts that under certain conditions contact planarity of one or more cantilevers is unachievable. This is due to the high torsional stiffness compared to the longitudinal bending stiffness. Third, in certain cases tip tangency of the lowest cantilever may be achieved before tip planarity. This means that there are design constraints—modelling can predict this. Fourth, the modelling has demonstrated the impact of tilt error on the tip/surface contact forces in different cantilevers. The tilt error results in a 'differential contact force error' or 'DCFE'—this can have an impact on the quality of electrical contacts. An experimental scale model probe based on three cantilevers gave results which agree well with the predictions of the model. The experimental work also enabled the observation of a small 'twist error' in a single cantilever—this is not accounted for in the modelling. Finally, for emerging automated electrical probing using MEMS devices, these newly identified and quantified effects could be compensated for using more involved numerical modelling (for specific probe geometries) combined with original

integrated sensing and feedback—enabling optimum automatic electrical contacting of miniature probes.

Acknowledgements

The work was carried out in support of the French ANR 'PRECISE' project.

Data availability statement

All the data are available in the manuscript. The data that support the findings of this study are available upon reasonable request from the authors.

ORCID iD

Steve Arscott https://orcid.org/0000-0001-9938-2683

References

[1] Chen L, Zhang C, Reck T J, Arsenovic A, Bauwens M, Groppi C, Lichtenberger A W, Weikle R M and Barker N S 2012 Terahertz Micromachined On-Wafer Probes: Repeatability and Reliability *IEEE Trans. Microwave Theory Techn.* **60** 2894–902

[2] Marzouk J, Arscott S, Fellahi A E, Haddadi K, Lasri T, Christophe Boyaval and Dambrine G 2015 MEMS probes for on-wafer RF microwave characterization of future microelectronics: design, fabrication and characterization *J. Micromech. Microeng.* **25** 075024

[3] Strid E 1997 A History of Microwave Wafer Probing *50th ARFTG Conference Digest* 50th ARFTG Conference Digest (Portland, OR, USA: IEEE) pp 27–34

[4] Wartenberg S A 2003 Selected topics in rf coplanar probing *IEEE Trans. Microwave Theory Techn.* **51** 1413–21

[5] Rumiantsev A and Doerner R 2013 RF Probe Technology: History and Selected Topics *IEEE Microwave* **14** 46–58

[6] Daffe K, Marzouk J, Boyaval C, Dambrine G, Haddadi K and Arscott S 2022 A comparison of pad metallization in miniaturized microfabricated silicon microcantilever-based wafer probes for low contact force low skate on-wafer measurements *J. Micromech. Microeng.* **32** 015007

[7] Sakamaki R and Horibe M 2018 Proposal of a Precision Probe-Tilt Adjustment with the RF Signal Detection Technique *2018 Conference on Precision Electromagnetic Measurements (CPEM 2018)* 2018 Conference on Precision Electromagnetic Measurements (CPEM 2018) (Paris: IEEE) pp 1–2

[8] Sakamaki R and Horibe M 2022 In-situ automatic adjustment of probe positions and tilt angles for GSGSG probe *2021 51st European Microwave Conference (EuMC)* 2021 51st European Microwave Conference (EuMC) (London, United Kingdom: IEEE) pp 789–92

[9] Kleist-Retzow F T von, Tiemerding T, Elfert P and Haenssler O C 2016 Automated Calibration of RF On-Wafer Probing and Evaluation of Probe Misalignment Effects Using a Desktop Micro-Factory *JCC* **04** 61–7

[10] Li H, von Kleist-Retzow F T, Haenssler O C, Fatikow S and Zhang X 2019 Multi-target tracking for automated RF on-wafer probing based on template matching *2019 International Conference on Manipulation, Automation and Robotics at Small Scales (MARSS)* 2019 International Conference on Manipulation, Automation and Robotics at Small Scales (MARSS) (Helsinki, Finland: IEEE) pp 1–6

[11] von Kleist-Retzow F T, Haenssler O C and Fatikow S 2016 Simulation of probe misalignment effects during RF on-wafer probing *2016 41st International Conference on Infrared, Millimeter, and Terahertz waves (IRMMW-THz)* 2016 41st International Conference on Infrared, Millimeter, and Terahertz waves (IRMMW-THz) (Copenhagen, Denmark: IEEE) pp 1–2

[12] Phung G N and Arz U 2020 Parasitic Probe Effects in Measurements of Coplanar Waveguides with Narrow Ground Width *2020 IEEE 24th Workshop on Signal and Power Integrity (SPI)* 2020 IEEE 24th Workshop on Signal and Power Integrity (SPI) (Cologne, Germany: IEEE) pp 1–4

[13] Phung G N, Schmuckle F J, Doerner R, Kahne B, Fritzsch T, Arz U and Heinrich W 2019 Influence of Microwave Probes on Calibrated On-Wafer Measurements *IEEE Trans. Microwave Theory Techn.* **67** 1892–900

[14] Votsi H, Urbonas J, Iezekiel S and Aaen P H 2021 Electromagnetic Field Measurements Above On-Wafer Calibration Standards *2021 96th ARFTG Microwave Measurement Conference (ARFTG)* 2021 96th ARFTG Microwave Measurement Conference (ARFTG) (San Diego, CA, USA: IEEE) pp 1–5

[15] Arscott S 2022 On overtravel and skate in cantilever-based probes for on-wafer measurements *J. Micromech. Microeng.* **32** 057001

[16] Arscott S 2022 Skate, overtravel, and contact force of tilted triangular cantilevers for microcantilever-based MEMS probe technologies *Sci Rep* **12** 19386

[17] Arscott S 2023 Quantifying and correcting tilt-related positioning errors in microcantilever-based microelectromechanical systems probes *J. Micromech. Microeng.* **33** 065008

[18] El Fellahi A, Haddadi K, Marzouk J, Arscott S, Boyaval C, Lasri T and Dambrine G 2015 Nanorobotic RF probe station for calibrated on-wafer measurements *2015 European Microwave Conference (EuMC)* 2015 European Microwave Conference (EuMC 2015) (Paris, France: IEEE) pp 163–6

[19] Taleb A, Pomorski D, Boyaval C, Arscott S, Dambrine G and Haddadi K 2020 Control and Automation for Miniaturized Microwave GSG Nanoprobing *Machine Vision and Navigation* ed O Sergiyenko, W Flores-Fuentes and P Mercorelli (Cham: Springer International Publishing) pp 751–68

[20] Slade P G 2014 *Electrical contacts: principles and applications* (Boca Raton, Fla.: CRC Press)

[21] Arscott S 2023 Corrigendum: On overtravel and skate in cantilever-based probes for on-wafer measurements (2022 J. Micromech. Microeng. 32 057001) *J. Micromech. Microeng.* **33** 099501

[22] Liu J-L, Feng X-Q, Xia R and Zhao H-P 2007 Hierarchical capillary adhesion of microcantilevers or hairs *J. Phys. D: Appl. Phys.* **40** 5564–70

[23] Young W C and Budynas R G 2002 *Roark's formulas for stress and strain* (New York: McGraw-Hill)

[24] Schneider C A, Rasband W S and Eliceiri K W 2012 NIH Image to ImageJ: 25 years of image analysis *Nat Methods* **9** 671–5

[25] Carolina Sparavigna A 2015 An Image Processing Approach Based on Gnu Image Manipulation Program Gimp to the Panoramic Radiography *ijSciences* **1** 57–67

[26] Whitt P 2023 Sharpening Images *Beginning Photo Retouching and Restoration Using GIMP* (Berkeley, CA: Apress) pp 287–98